

# Comparison of hyperfine anomalies in the $5S_{1/2}$ and $6S_{1/2}$ levels of $^{85}\text{Rb}$ and $^{87}\text{Rb}$ .

A. Pérez Galván<sup>a</sup> Y. Zhao<sup>a</sup> L. A. Orozco<sup>a,\*</sup> E. Gómez<sup>b,1</sup>  
A. D. Lange<sup>b,2</sup> F. Baumer<sup>b,3</sup> G. D. Sprouse<sup>b</sup>

<sup>a</sup>*Joint Quantum Institute, Department of Physics, University of Maryland and National Institute of Standards and Technology, College Park, MD 20742-4100, USA.*

<sup>b</sup>*Department of Physics and Astronomy, SUNYSB, Stony Brook NY 11794-3800, USA.*

---

## Abstract

We observe a hyperfine anomaly in the measurement of the hyperfine splitting of the  $6S_{1/2}$  excited level in rubidium. We perform two step spectroscopy using the  $5S_{1/2} \rightarrow 5P_{1/2} \rightarrow 6S_{1/2}$  excitation sequence. We measure the splitting of the  $6S_{1/2}$  level and obtain for the magnetic dipole constants of  $^{85}\text{Rb}$  and  $^{87}\text{Rb}$   $A = 239.18(4)$  MHz and  $A = 807.66(8)$  MHz, respectively. The hyperfine anomaly difference of  $_{87}\delta_{85} = -0.0036(2)$  comes from the Bohr Weisskopf effect: a correction to the point interaction between the finite nuclear magnetization and the electrons, and agrees with that obtained in the  $5S_{1/2}$  ground state.

*Key words:*

Hyperfine anomaly, Precision Spectroscopy, Nuclear Structure

PACS: 21.60.-n, 32.10.Fn, 32.30.-r

---

Measurements of hyperfine splittings provide a low energy approach to study the magnetic moment distribution in the nucleus. The hyperfine splitting is due mainly to the coupling between the magnetization of the nucleus with the magnetic field created by the electrons. To a very good approximation

---

\* Corresponding Author

*Email address:* [lorozco@umd.edu](mailto:lorozco@umd.edu) (L. A. Orozco).

<sup>1</sup> Present address: Instituto de Física, Universidad Autónoma de San Luis Potosí, SLP, México.

<sup>2</sup> Present address: Institut für Experimentalphysik, Universität Innsbruck, Austria.

<sup>3</sup> Present address: Institut für Experimentalphysik, Heinrich-Heine-Universität Düsseldorf, Germany.

the coupling is taken to be point-like. However, high precision measurements of the splitting can reveal deviations from the point interaction. These deviations, also called hyperfine anomalies, come from considering how finite magnetic and charge distributions affect the interaction. Bohr and Weisskopf [1] first discussed the finite magnetization effect in the anomaly. The modified charge potential that the valence electron sees as it gets closer to the nucleus, the Breit-Crawford-Rosenthal-Schawlow [2,3] effect, is the other source for a hyperfine anomaly.

We show in this letter a measurement of the excited state hyperfine splittings in two isotopes precise enough to extract a difference in the hyperfine anomalies. The hyperfine anomaly differences of the ground state in francium were measured by our group [4] by comparing the ratio of the hyperfine splittings of the  $7P_{1/2}$  (which has a small anomaly) and the  $7S_{1/2}$  (which has the large anomaly) [5]. These measurements represent excellent benchmarks to test state-of-the-art *ab initio* calculations of the electronic and nuclear wave functions for future parity non-conservation measurements [6,7]. They give the possibility to look at how the systematic addition of a neutron modifies the electronic wavefunction in the nucleus, and how the nucleus rearranges itself. As a new generation of proposed parity violation experiments in atoms starts, [6,8,9], it is important to understand the nuclear structure limiting factors for the extraction of weak coupling parameters from the measurements [10]. This letter presents a new experimental approach to extract and study such effects in chains of isotopes.

The hyperfine shift for these levels is given by  $E_{HF} = A(F(F+1) - I(I+1) - J(J+1))/2$  where  $A$  is the magnetic dipole constant,  $F$  is the total angular momentum,  $I$  is the nuclear spin, and  $J$  is the total electronic angular momentum. Derivations of  $A$  assume that the nucleus is a point particle with magnetic moment  $\mu_N$  and charge  $Z$ . However, this is not the case. The nucleus has a finite extension and structure. The value of the magnetic dipole constant has to be modified to include the effect of the charge and magnetic distribution on the electronic wave function. We can write, following Ref. [11]  $A$  for an extended (*ext*) nucleus as a function of the point value (*point*) (Eq. 1):

$$A_{point} = \frac{16\pi}{3} \frac{\mu_0}{4\pi\hbar} g_I \mu_N \mu_B |\psi(0)|^2 f_R,$$

$$A_{ext} = A_{point} (1 + \epsilon_{BCRS}) (1 + \epsilon_{BW}), \quad (1)$$

where  $\psi(0)$  is the electronic wave function evaluated at the center of the nucleus,  $\mu_B$  is the Bohr magneton,  $\mu_N$  is the nuclear magneton,  $g_I$  is the nuclear g-factor, and  $f_R$  represents the relativistic enhancement. The last two terms of this expression modify the hyperfine interaction to account for an extended nucleus. The first of them ( $\epsilon_{BCRS}$ ), the Breit-Crawford-Rosenthal-Schawlow (BCRS) correction, accounts for the fact that the valence electron sees a mod-

ified potential as it gets closer to the nucleus. The second one ( $\epsilon_{BW}$ ), the Bohr Weisskopf (BW) effect, focuses on the magnetic distribution of the nucleus.

The fractional difference in the mean charge radius between the two isotopes of interest ( $^{85}\text{Rb}$  and  $^{87}\text{Rb}$ ) is less than  $10^{-3}$  and justifies neglecting the BCRS correction [12,13].  $^{87}\text{Rb}$  has a closed-neutron shell that makes the nuclear charge distribution insensitive to the addition or subtraction of neutrons [12]. A calculation of  $\epsilon_{BCRS}$  [14] gives a value of 1% compared to the point nucleus; however, since we are interested in comparing the two anomalies we find, using the values of the charge radius of Ref. [13], the difference between the corrections of both isotopes is less than  $10^{-4}$ .

The BW correction describes the modification of the hyperfine interaction due to a finite distribution of nuclear magnetization. The addition of more neutrons to the nucleus yields a different spatial magnetization. The magnitude of this correction for an individual nucleus is smaller than the BCRS correction but depends heavily on the spin and orbital angular momentum of the nucleus and not just on its radius. For the particular case of  $^{85}\text{Rb}$  and  $^{87}\text{Rb}$  the addition of two neutrons changes the value of the valence proton from an  $f_{5/2}$  orbital to a  $p_{3/2}$  orbital. The lighter of the isotopes,  $^{85}\text{Rb}$ , has the spin angular momentum of the valence proton anti-aligned with its orbital angular momentum while  $^{87}\text{Rb}$  adds them both together. The two neutron holes deform the nucleus very slightly and change the order of the orbitals that are almost degenerate. The difference of the hyperfine anomaly contributions  $_{87}\delta_{85} = \epsilon_{BW}^{87} - \epsilon_{BW}^{85}$  is dominated by the BW contribution as we take the BCRS correction as equal for both isotopes.

Since the magnetic moments of the nuclei are well known [15] we can use a ratio to extract the Bohr-Weisskopf effect difference:

$$\frac{A^{87}g^{85}}{A^{85}g^{87}} \simeq 1 + _{87}\delta_{85}. \quad (2)$$

Because the BW corrections are small, we require a method to measure the hyperfine splitting with good precision. We perform two-photon absorption spectroscopy in a 30 cm long 2.5 cm diameter Rb cell with natural isotopic abundances to measure the hyperfine splitting of the  $6S_{1/2}$  level using the  $5P_{1/2}$  as an intermediate level (see Fig. 1 for the block diagram of the experimental setup and the atomic energy levels involved). The cell has no buffer gas and is in a controlled magnetic environment.

We monitor the change in absorption of a laser resonant with the transition to the  $5P_{1/2}$  level at 795 nm as we scan the 1.3  $\mu\text{m}$  laser over the hyperfine structure of the  $6S_{1/2}$  level. We modulate the 1.3  $\mu\text{m}$  laser at a frequency close to half of the hyperfine separation to produce sidebands well separated

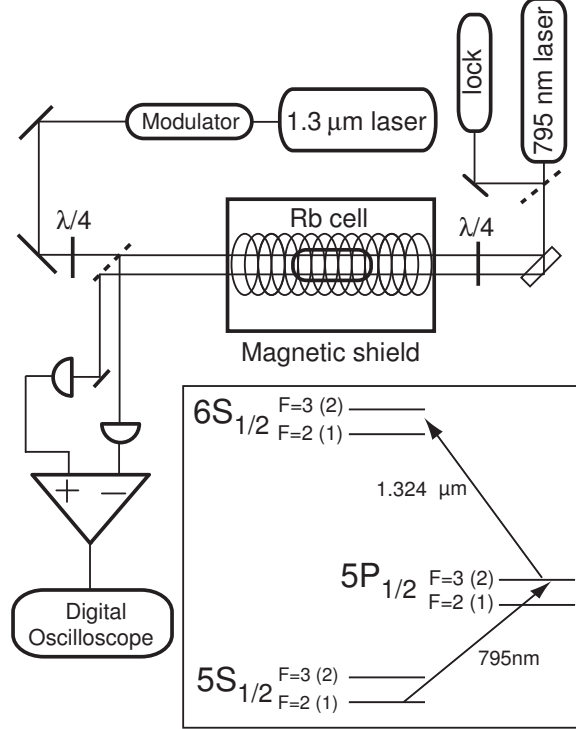


Fig. 1. Schematic of the experimental apparatus. The inset shows the energy levels relevant to our experiment (not drawn to scale) with quantum numbers corresponding to  $^{85}\text{Rb}$  ( $^{87}\text{Rb}$ ).

in energy. This way we only need to scan the laser a small range around the midpoint between the two hyperfine levels of the  $6S_{1/2}$  level such that the sidebands scan over both hyperfine levels. The sideband signals appear in the absorption profile and work as an *in situ* scale. We record absorption profiles at different values for the modulation to find, with the help of linear regression plots, the point where the sidebands cross the midpoint of the two main peaks. Typical fits give correlation coefficients that differ from unity by at most  $2 \times 10^{-4}$ .

A Titanium Sapphire laser with a linewidth better than 500 kHz tuned to the Rb  $D_1$  line at 795 nm excites the first step of the transition. A Pound-Drever-Hall setup on an independent Rb cell locks the 795 nm laser to the  $F=1(2) \rightarrow F'=2(3)$  transition in  $^{87}\text{Rb}$  ( $^{85}\text{Rb}$ ). A grating narrowed diode laser at 1.324  $\mu\text{m}$  with a linewidth better than 500 kHz excites the second transition. We scan the frequency of the 1.3  $\mu\text{m}$  laser using a triangular shaped voltage ramp from a synthesized function generator at 4 Hz applied to the piezo control of the grating and monitor its frequency with a wavemeter. A fiber-coupled semiconductor optical amplifier increases the power of the 1.3  $\mu\text{m}$  laser before it goes to a large bandwidth ( $\approx 10$  GHz) Electro-Optic Modulator (EOM). A signal generator modulates this EOM in the range between 100 and 900 MHz to imprint the sidebands necessary for the measurement.

Before going through the rubidium vapor cell the laser beams are circularly polarized by  $\lambda/4$  waveplates. A counter propagating  $1.3\ \mu\text{m}$  laser beam with a power of up to 4 mW overlaps one of the 795 nm beams. The relative power on the sidebands is less than a tenth of the total and its waist is 1 mm. The lasers overlap to a precision of better than 1 mm along 75 cm. The cell resides in the center of a 500-turn solenoid (7.4 Gauss/A) contained inside a three layered magnetic shield. The solenoid is 70 cm long and has a diameter of 11.5 cm.

A thick glass plate splits the 795 nm laser beam into two co-propagating beams. The power of each beam is approximately  $10\ \mu\text{W}$  with a waist of 1 mm. We find that doing the two step excitation in either a  $(\sigma^+, \sigma^-)$  or  $(\sigma^-, \sigma^+)$  polarization sequence for the 795 nm and  $1.3\ \mu\text{m}$  lasers respectively, increases the probability of the transition to the  $6S_{1/2}$  level, and allows us to check for optical pumping and Zeeman shift effects. We place the Rb cell in a uniform magnetic field convenient for the  $\Delta m_F = \pm 1$  transitions. The addition of the magnetic field has the two-fold advantage of providing a quantization axis and a tool to probe systematic effects. We measure the hyperfine splitting for different values, including reversals, of the magnetic field and polarization. We can then extract by interpolation the value of the hyperfine splitting at zero magnetic field.

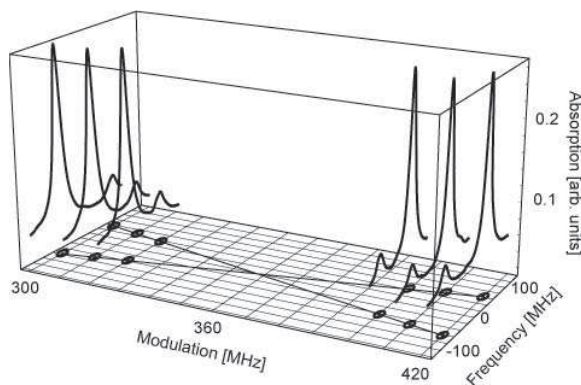


Fig. 2. Experimental traces that illustrate sideband crossing for  $^{85}\text{Rb}$ . The intersection of the two projected lines marks half the hyperfine separation.

After the glass cell an independent photodiode detects each 795 nm laser beam. The output of both detectors goes to a differential amplifier to reduce common noise. A digital storage oscilloscope records the signal and averages for about three minutes. The stability of the  $1.3\ \mu\text{m}$  laser center frequency over this time is better than 0.3 MHz as measured by a Fabry Perot cavity. The optical attenuation at line center ( $D_1$  line) is 0.4 for  $^{85}\text{Rb}$ . Fig. 2 presents an example of the oscilloscope traces for different sideband frequencies. The projection shows the positions of the peaks joined by the linear interpolation, the error in the position is much smaller than the dots. We obtain signal to noise ratios in excess of 100 for the sideband resonances.

We analyze how the following parameters influence the hyperfine separation: the peak shape model for the non-linear fit to obtain the separation of the centers of the lines, scan width and repetition rate of the 1.3  $\mu\text{m}$  laser, power of the 795 nm and 1.3  $\mu\text{m}$  lasers. We look for optical pumping effects, magnetic field effects, and temperature, though the vapor density, that can influence the hyperfine separation. We have only been able to put upper bounds on the systematic shifts within our resolution and we determine that statistical fluctuations, as stated by the standard error of the mean, dominate the uncertainty of the hyperfine splitting ( $\nu_{HF}$ ) measurement as seen in Table 1.

Table 2 presents the results of the hyperfine splitting of the  $6S_{1/2}$  level as well as the corresponding values of the magnetic dipole constants for both isotopes. Our results are consistent with the past measurements of Gupta *et al.* [17] and represent a precision improvement by a factor of 63 for  $^{87}\text{Rb}$  and by a factor of 30 for  $^{85}\text{Rb}$ . The table contains the theoretical predictions for  $^{85}\text{Rb}$  of Safronova *et al.* [16]. The theoretical calculation includes corrections for the finite size of the nuclear magnetic moment distribution, which is modelled as a uniformly magnetized ball. The theory value for  $^{87}\text{Rb}$  comes from multiplying the theoretical value of the splitting in  $^{85}\text{Rb}$  by the ratio of nuclear gyromagnetic ratios and does not include a hyperfine anomaly difference.

Optical pumping effects are the most delicate of all the systematic effects. The polarization of the lasers determine the relative sizes of the peaks ( $m$  sublevels) that form the resonances of the  $6S_{1/2}$  hyperfine levels. For our experimental conditions (around 1 G with circularly polarized light) we observe no difference between positive and negative magnetic field directions. Table 1 shows the bound for this effect.

Systematic effects	$\nu_{HF}(^{85}\text{Rb})$ (MHz)	$\nu_{HF}(^{87}\text{Rb})$ (MHz)
Optical pumping effects	$\leq 0.016$	$\leq 0.029$
Power of 795 nm laser	$\leq 0.020$	$\leq 0.005$
Power of 1.3 $\mu\text{m}$ laser	$\leq 0.011$	$\leq 0.011$
Atomic density	$\leq 0.020$	$\leq 0.010$
Non linear fit	$\leq 0.028$	$\leq 0.023$
B-field fluctuations	$\leq 0.015$	$\leq 0.025$
Total Systematic	$\leq 0.047$	$\leq 0.047$
Statistical error	0.100	0.160
<b>TOTAL</b>	<b>0.110</b>	<b>0.167</b>

Table 1  
Error budget for the hyperfine splitting measurement

	$^{85}\text{Rb}$ [MHz]	$^{87}\text{Rb}$ [MHz]
$\nu_{HF}$ this experiment	717.540(110)	1615.320(167)
$A$ previous experiment [17]	239.3(12)	809.1(50)
$A$ this experiment	239.18(4)	807.66(8)
$A$ theory [16]	238.2	807.3

Table 2

Hyperfine splittings and magnetic dipole constants for the  $6S_{1/2}$  level.

We change the power of the 795 nm and 1.3  $\mu\text{m}$  lasers to look for any kind of dependence that would indicate line splitting effects such as the Autler-Townes effect or power broadening. We observe no systematic variation in the hyperfine separation as a function of laser powers. No systematic effect is found in the hyperfine splitting for changes in the temperature of the cell from 23 to 40  $^{\circ}\text{C}$ . The bounds for these effects are on Table 1.

The observed linewidths range from 30 to 40 MHz and fit (reduced  $\chi^2$ ) Lorentzian profiles better ( $\approx 1$ ) than Gaussian ( $\approx 10$ ), with the Voigt profile between the two. We do not observe changes in the splitting that depend on the frequency range fitted around the resonances. The values obtained for the difference between the centers of the resonances using Gaussian fits give consistent results with the Lorentzian fits, not changing the measured splitting by more than the reported error.

The three layers of magnetic shielding limit the external magnetic fluctuations to less than 1 mG, while the stability of the magnetic field from the solenoid is comparable. We operate within the low magnetic field regime (1 G) and extrapolate to  $B=0$  for both polarization sequences with linear fits with an average correlation coefficient of 0.97.

Figure 3 shows the normalized ratio of hyperfine constants from Eq. 2 to show the hyperfine anomaly difference extracted from our measurement in the  $6S_{1/2}$  level of  $^{85}\text{Rb}$  and  $^{87}\text{Rb}$  as well as the corresponding values for other levels currently in the literature. We use the values from Duong *et al.* [15] to obtain the ratio of  $g$  values  $g_{85}/g_{87} = 0.295061 \pm 0.00003$ , which is consistent with the values quoted by Stone [18], to calculate the hyperfine anomaly difference from the measured  $A$  coefficients. The hyperfine splittings of the  $5S_{1/2}$  ground state are very well known as they are used in atomic clocks [19]. The  $5P_{1/2}$  ratio comes from the work of Barwood *et al.* [20] which is consistent with more recent frequency comb measurements [21,22]. The  $6S_{1/2}$  ratio corresponds to the present measurement which gives  $_{87}\delta_{85}(6S_{1/2}) = -0.0036(2)$ . The difference in the anomalies is indeed a factor of thirty larger than the expected BCRS contribution and it comes from the BW effect. The  $6P_{1/2}$  ratio comes from the critical evaluation of Arimondo *et al.* [19], while we find

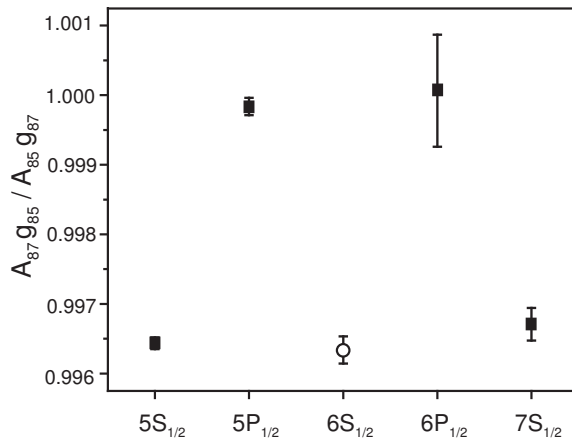


Fig. 3. Ratio of hyperfine constants normalized by the nuclear g factors showing hyperfine anomaly differences in  $^{85}\text{Rb}$  and  $^{87}\text{Rb}$  based on five different electronic states. The value for the  $6S_{1/2}$  (circle) comes from the present measurement. See the text for the other references (squares).

from the recent frequency comb measurement of the  $7S_{1/2}$  state by Chui *et al.* [23]  $_{87}\delta_{85}(7S_{1/2}) = -0.0033(2)$ , although they do not calculate nor mention the hyperfine anomaly in their paper. We have not been able to find in the literature values for higher levels with adequate precision to include them in the figure. Fig. 3 shows that the hyperfine anomaly difference measured with the  $S_{1/2}$  states is independent of the principal quantum number, just as Bohr and Weisskopf predicted [1]. The measurements are consistent with each other as are the  $P_{1/2}$  states that show a much smaller anomaly.

We have measured the hyperfine splittings of the  $6S_{1/2}$  level of  $^{85}\text{Rb}$  and  $^{87}\text{Rb}$  to a precision of 153 ppm and 103 ppm, respectively. Our measurement allows us to extract the hyperfine anomaly difference of the two isotopes with a precision of 5%. It is in excellent agreement with that of the ground state, confirming that it is the angular momentum and not the principal quantum number that enters in the Bohr Weisskopf effect [1]. We show also that nuclear magnetization information can be extracted through careful probing of excited state hyperfine splittings.

Work supported by NSF. E. G. acknowledges support from CONACYT.

## References

- [1] A. Bohr, V. F. Weisskopf, Phys. Rev. 77 (1950) 94.
- [2] J. E. Rosenthal, G. Breit, Phys. Rev. 41 (1932) 459.
- [3] M. F. Crawford, A. L. Schawlow, Phys. Rev. 76 (1949) 1310.



- [4] J. S. Grossman, L. A. Orozco, M. R. Pearson, J. E. Simsarian, G. D. Sprouse, W. Z. Zhao, Phys. Rev. Lett. 83 (1999) 935.
- [5] J. R. Persson, Eur. Phys. J. A 2 (1998) 3.
- [6] E. Gomez, L. A. Orozco, G. D. Sprouse, Rep. Prog. Phys. 66 (2006) 79.
- [7] E. Gomez, S. Aubin, L. A. Orozco, G. D. Sprouse, D. DeMille, Phys. Rev. A 75 (2007) 033418.
- [8] M.-A. Bouchiat, C. Bouchiat, Rep. Prog. Phys. 60 (1997) 1351.
- [9] M. A. Bouchiat, Phys. Rev. Lett. 98 (2007) 043003.
- [10] A. Derevianko, S. G. Porseu, Phys. Rev. A 65 (2002) 052115.
- [11] H. Kopfermann, Nuclear Moments, Academic Press, New York, 1958.
- [12] C. Thibault, F. Touchard, S. Büttgenbach, R. Klapisch, M. de Saint Simon, H. T. Duong, P. Jacquinet, P. Juncar, S. Liberman, P. Pillet, J. Pinard, J. L. Vialle, A. Pesnelle, G. Huber, Phys. Rev. C 23 (1981) 2720.
- [13] I. Angeli, At. Data Nucl. Data Tables 87 (2004) 185.
- [14] L. Armstrong Jr, Theory of the Hyperfine Structure of Free Atoms, Wiley-Interscience, New York, 1971.
- [15] H. T. Duong, C. Ekström, M. Gustafsson, T. T. Inamura, P. Juncar, P. Lievens, I. Lindgren, S. Matsuki, T. Murayama, R. Neugart, T. Nilsson, T. Nomura, M. Pellarin, S. Penselin, J. Persson, J. Pinard, I. Ragnarsson, O. Redi, H. H. Stroke, J. L. Vialle, the ISOLDE Collaboration, Nuc. Instr. and Meth. A 325 (1993) 465.
- [16] M. S. Safronova, W. R. Johnson, A. Derevianko, Phys. Rev. A 60 (1999) 4476.
- [17] R. Gupta, W. Happer, L. K. Lam, S. Svanberg, Phys. Rev. A 8 (1973) 2792.
- [18] N. J. Stone, At. Data Nucl. Data Tables 90 (2005) 75.
- [19] E. Arimondo, M. Inguscio, P. Violino, Rev. Mod. Phys. 49 (1977) 31.
- [20] G. P. Barwood, P. Gill, W. R. C. Rowley, Appl. Phys. B: Photophys. Laser Chem. 53 (1991) 142.
- [21] A. Marian, M. C. Stowe, J. R. Lawall, D. Felinto, J. Ye, Science 306 (2004) 2063.
- [22] A. Marian, M. C. Stowe, D. Felinto, J. Ye, Phys. Rev. Lett. 95 (2005) 023001.
- [23] H.-C. Chui, M.-S. Ko, Y.-W. Liu, J.-T. Shy, J.-L. Peng, H. Ahn, Opt. Lett. 30 (2005) 842.